# Research Article

# X-ray photoelectron spectroscopic chemical state quantification of mixed nickel metal, oxide and hydroxide systems

## Mark C. Biesinger,[a,b]* Brad P. Payne,[c] Leo W. M. Lau,[a,c] Andrea Gerson[b] and Roger St. C. Smart[b]

Quantitative chemical state X-ray photoelectron spectroscopic analysis of mixed nickel metal, oxide, hydroxide and oxyhydroxide systems is challenging due to the complexity of the Ni 2p peak shapes resulting from multiplet splitting, shake-up and plasmon loss structures. Quantification of mixed nickel chemical states and the qualitative determination of low concentrations of Ni(III) species are demonstrated via an approach based on standard spectra from quality reference samples (Ni, NiO, Ni(OH)$_2$, NiOOH), subtraction of these spectra, and data analysis that integrates information from the Ni 2p spectrum and the O 1s spectra. Quantification of a commercial nickel powder and a thin nickel oxide film grown at 1-Torr O$_2$ and 300 °C for 20 min is demonstrated. The effect of uncertain relative sensitivity factors (e.g. Ni 2.67 ± 0.54) is discussed, as is the depth of measurement for thin film analysis based on calculated inelastic mean free paths. Copyright © 2009 John Wiley & Sons, Ltd.

## Introduction

The interpretation and quantification of transition metal chemical states from the metal 2p XPS envelope are recognized to carry a high degree of uncertainty due to the complex, extended multiplet, shake-up and plasmon loss structures and are further confounded by overlap between the various chemical states. Binding energy databases, such as the National Institute of Standards and Technology (NIST) Database[1] or the Phi Handbook[2] attempt to assign oxidation states from the binding energies of the 2p$_{3/2}$ signal assuming a single identifiable peak maximum. This assumption has been shown to be invalid for many transition metal spectra, e.g. Cr,[3] Mn,[4,5] Fe,[6] and Ni.[7] Assignment of the multiplet envelope and other structures to each chemical state is necessary for quantitative speciation analysis and is vital for the analysis relevant to processing of materials, minerals, ceramics and many other technologies.

Grosvenor et al.[7] present an investigation of the multiplet splitting structure of the Ni(OH)$_2$, NiOOH and NiO Ni 2p spectra and the plasmon loss structure associated with metal Ni 2p spectrum. Plasmon loss features must be included in any quantitative analysis that includes metallic Ni. Analysis of EELS[8] and REELS[7] data has been used to assign the surface and bulk plasmons within the Ni metal 2p XPS spectrum. Ni(OH)$_2$ and NiOOH were found to fit reasonably to the multiplet line shape initially calculated for the free ions by Gupta and Sen.[9,10] NiO, which shows a well-resolved set of peaks, could only be satisfactorily fitted with the Gupta and Sen line shape by allowing variation in the binding energy positions of the multiplet contributions. For all three compounds, a broad peak associated with other intrinsic losses at a higher binding energy than the main peak multiplets, must be added to model the valley between the main peak and the satellite structures as is consistent with the inter-band losses attributed by Hagelin-Weaver et al.[8,11]

Roberts and Smart[12] have investigated changes in the defect structure of NiO due to heat treatment. A peak at 856.1 eV, detectable through the application of shallow takeoff angle analysis, was attributed to the presence of Ni(III). Ni(III) has also been shown to be present within a K doped Ni(110)-O surface.[13] Spectral subtractions have been used[13,14] to identify the presence of Ni(III) within the complex spectral profile of NiO of thin oxide films (<2 nm). Ni(III) compounds of β-NiOOH and 'nickel peroxide' have been shown to be chemically identical[15] with conversion of both, in vacuum, to defective NiO at 773 K.

McIntyre et al.[16] applied spectra of standard NiO and NiFe$_2$O$_4$ to the study Inconel 600 alloys under very mild oxidation conditions. Matienzo et al.[17] present a survey of analyses of numerous nickel compounds (including a large number of nickel complexes) and give single positions for both the 2p$_{3/2}$ and 2p$_{1/2}$ peaks.[18] The spectra presented show the presence of multiplet structures and shake-up satellites. In recognition of the multicomponent basis of the Ni 2p spectra from the metal, oxide, oxyhydroxide and hydroxide, the objective of the study presented herein is to provide a self-consistent and easily operable basis for fitting spectral combinations of these species to obtain quantitative estimates of their contributions.

*   Correspondence to: Mark C. Biesinger, Surface Science Western, Room G1, Western Science Centre, The University of Western Ontario, London, Ontario, Canada N6A 5B7, Canada. E-mail: biesingr@uwo.ca

a   Surface Science Western, Room G1, Western Science Centre, The University of Western Ontario, London, Ontario, Canada N6A 5B7, Canada

b   ACeSSS (Applied Centre for Structural and Synchrotron Studies), University of South Australia, Mawson Lakes, SA 5095, Australia

c   Department of Chemistry, The University of Western Ontario, London, Ontario, N6A 5B7, Canada

## Experimental

The XPS analyses were carried out with a Kratos Axis Ultra spectrometer using a monochromatic Al K$\alpha$ source (15 mA, 14 kV). The instrument work function was calibrated to give an Au $4f_{7/2}$ metallic gold binding energy of 83.95 eV. The spectrometer dispersion was adjusted to give a binding energy of 932.63 eV for metallic Cu $2p_{3/2}$. The Kratos charge neutralizer system was used for all the analyses. Instrument base pressure is $8 \times 10^{-10}$ Torr. High-resolution spectra were obtained using either a 10- or 20-eV pass energy, an analysis area of $\approx 300 \times 700$ μm, 50-meV step and 60-s sweep intervals. For Ni 2p, O 1s and C 1s, binding energy ranges and total number of sweeps are as follows: 848–890 eV, 50–75 sweeps; 525–540 eV, 5–10 sweeps; 278–295 eV, 5–10 sweeps; respectively. The average analysis time for one sample spot is 1.5–2 h.

The C 1s spectrum for adventitious C was fit by defining a peak constrained to be 1.5 eV above the main peak, of equal full width half maxima (FWHM) to the main peak (C–C, C–H). This higher binding energy peak is ascribed to alcohol and/or ester functionality. Further, high binding energy components were added if required. Spectra from insulating samples have been charge corrected to obtain the adventitious C 1s spectral component binding energy of 284.8 eV. The process has an associated error of at least $\pm 0.1$ to $\pm 0.2$ eV.[19] Experience with numerous conducting samples and a routinely calibrated instrument have shown that the C 1s signal generally ranges from 284.7 eV to as high as 285.2 eV [M.C. Biesinger, unpublished results]. The Ni metal spectrum is corrected to Au $4f_{7/2}$ at 83.95 eV.

Spectra were analyzed using CasaXPS software[20] (version 2.3.14). Gaussian (70%)–Lorentzian (30%), defined in CasaXPS as GL(30), profiles were used for each component. Asymmetry of the main metal peak was defined in the form of LA ($\alpha$, $\beta$, $m$) where $\alpha$ and $\beta$ define the spread of the tail on either side of the Lorentzian component. The parameter $m$ specifies the width of the Gaussian used to convolute the Lorentzian curve. If values of $\alpha$ and $\beta$ greater than unity are used, this line shape will correct a problem with previous asymmetric line shapes[3,6,7] that tend to incorrectly estimate the peak area by incorporating area under the curve from binding energies well above the peak profile[20] [N. Fairley, personal communication].

A standard Shirley background is used for the reference sample spectra. A Shirley type baseline with varying amounts of offset at the high binding energy end point was used for fitting the mixed metal/oxide/hydroxide spectra. Values for this parameter can range from 0 to 5.

Ni metal (99.995% purity, rod), NiO (99.998%, Puratronic) and Ni(OH)$_2$ powder (61% Ni) were purchased from Alfa Aesar (Ward Hill, MA, USA). The metal was sputter etched with a 4 kV argon ion beam to remove all O and C contamination prior to analysis. The purity of the NiO samples was confirmed by energy dispersive X-ray (EDX) spectroscopy and by XRD. The purity of the Ni(OH)$_2$ samples was confirmed by EDX and by Fourier transform infrared (FTIR) spectroscopy. Fresh NiO was introduced into the XPS instrument via an argon-filled glove box. The preparation and characterization by XRD of $\gamma$-NiOOH and $\beta$-NiOOH have been reported previously.[7] The thin film oxide sample (Case 1) was prepared by exposing a polished and argon ion beam sputter cleaned pure nickel (99.995%) surface to 1-Torr O$_2$ at 300 °C for 20 min. The thin film oxide sample (Case 4) was prepared by exposing a polished and argon ion beam sputter cleaned pure nickel (99.995%) surface to 1-Torr O$_2$ at 300 °C for 1 min. Both thin

film samples were transferred in vacuum to the analysis chamber of the XPS instrument. The INCO (Type 123) nickel powder and ultrafine nickel powder samples were supplied by INCO Special Products (Canada). All powder samples were either pressed onto indium foil or mounted on a nonconductive adhesive tape.

## Results and Discussion

### Standard samples

NiO spectral analysis was based on four spectra (different samplings of the NiO standard powder sample) collected at 10-eV pass energy and three spectra collected at 20-eV pass energy. Ni(OH)$_2$ spectral analysis was based on four spectra collected at 10-eV pass energy and four spectra collected at 20-eV pass energy. Peak positions for NiO and Ni(OH)$_2$ have standard deviations of 0.06 and 0.14 eV, respectively. Ni metal spectral analysis was based on two spectra collected at 10-eV pass energy and two spectra collected at 20-eV pass energy. $\gamma$-NiOOH and $\beta$-NiOOH spectral analyses are derived from the data presented by Grosvenor *et al*.[7] A Shirley type background was utilized encompassing the Ni $2p_{3/2}$ peak only. Peak positions, FWHM, peak spacing and area percentages are presented in Table 1.

The Ni metal $2p_{3/2}$ peak position of 852.6 eV is within the literature value range of 852.7 eV $\pm$ 0.4 eV.[1] The metal Ni $2p_{3/2}$ peak does not broaden significantly between 10 eV and 20-eV pass energies (0.94- to 0.95-eV FWHM, respectively). The FWHM of the narrowest peak of the NiO spectrum also does not change significantly with pass energy (0.98 eV at 10-eV pass energy and 1.02 eV at 20-eV pass energy). This has also been shown to be the case for chromium compound XPS measurements where FWHM values for Cr$_2$O$_3$ were found to be 0.88 and 0.94 eV for 10- and 20-eV pass energies, respectively.[3] These results suggest that a higher pass energy (lower resolution) setting may be sufficient for most analyses, particularly when smaller amounts of analyte are present.

The NiO O 1s spectral component is found at 529.3 eV ($\pm$0.04 eV) with a FWHM of 0.85 and 0.92 eV for 10 and 20-eV pass energies. A major O 1s peak, approximately 30% of the total O 1s spectral area, at the binding energy of 531.1 eV ($\pm$0.04-eV FWHM $\approx$1.5 eV for both pass energies) has been proposed to be due to defective sites within the oxide crystal,[8,21,22] adsorbed oxygen,[23] or hydroxide species.[24] Recent work on oxide films grown by exposure to only O$_2$ suggests that this peak is likely to be due to defective sites within the NiO structure.[22] Other references concur with this assignment[8] including results from nuclear reaction analyses (NRA) that rule out the possibility of Ni(OH)$_2$ or NiOOH.[22] A small peak at 532.8 eV ($\pm$0.1 eV, FWHM constrained to that of the defective site peak at 531.1 eV) may be due to adsorbed water or possibly adsorbed O$_2$. For Ni(OH)$_2$, the O 1s with binding energy of 530.9 eV ($\pm$0.1 eV, FWHM of 1.46 eV for both pass energies) can be almost entirely ascribed to the hydroxide. O 1s spectra for NiO and Ni(OH)$_2$ are presented in Fig. 1.

### Case 1: Ni Metal with NiO

An example of the quantitative spectral fitting of a 3.3- $\pm$ 0.2-nm thick oxide film grown on a polished pure nickel metal substrate at 1-Torr O$_2$ and 300 °C for 20 min is shown in Fig. 2. Oxide thickness was obtained using the calculations in the 'depth of analysis' section and has been confirmed by QUASES and NRA analyses. The spectrum is fitted with the asymmetric line shape and plasmon

**S**URFACE *and* **I**NTERFACE **A**NALYSIS

M. C. Biesinger *et al.*

**Table 1.** Spectral fitting parameters for Ni $2p_{3/2}$: binding energy (eV), percentage of total area, FWHM value (eV) for each pass energy, and spectral component separation (eV)

| Compound | Peak 1 (eV)[a] | % | Peak 1, FWHM, 10-eV pass energy | Peak 1, FWHM, 20-eV pass energy | Δ Peak 2 – Peak 1 (eV)[a] | Peak 2 (eV) | % | Peak 2, FWHM, 10-eV pass energy | Peak 2, FWHM, 20-eV pass energy | Δ Peak 3 – Peak 2 (eV) | Peak 3 (eV) | % | Peak 3, FWHM, 10-eV pass energy | Peak 3, FWHM, 20-eV pass energy | Peak 4 (eV) | Δ Peak 4 – Peak 3 (eV) | % | Peak 4, FWHM, 10-eV pass energy | Peak 4, FWHM, 20-eV pass energy | |
|---|---|---|---|---|---|---|---|---|---|---|---|---|---|---|---|---|---|---|---|---|
| Ni metal from Ref. [7] | 852.6 | 79.6 | 1.00 | 1.02 | 3.65 | 856.3 | 5.6 | 2.48 | 2.48 | 2.38 | 858.7 | 14.8 | 2.48 | 2.48 | | | | | | bd |
| Ni metal – New line shape | 852.6 | 81.2 | 0.94 | 0.95 | 3.65 | 856.3 | 6.3 | 2.70 | 2.70 | 2.38 | 858.7 | 12.5 | 2.70 | 2.70 | | | | | | cd |
| NiO | 853.7 | 14.3 | 0.98 | 1.02 | 1.71 | 855.4 | 44.2 | 3.20 | 3.25 | 5.44 | 860.9 | 34.0 | 3.85 | 3.76 | 864.0 | 3.10 | 3.6 | 1.97 | 2.04 | |
| Ni(OH)2 | 854.9 | 7.4 | 1.12 | 1.16 | 0.77 | 855.7 | 45.3 | 2.25 | 2.29 | 2.02 | 857.7 | 3.0 | 1.59 | 1.59 | 860.5 | 2.79 | 1.4 | 1.06 | 1.06 | |
| Gamma NiOOH | 854.6 | 13.8 | 1.40 | | 0.70 | 855.3 | 12.4 | 1.50 | | 0.36 | 855.7 | 9.7 | 1.40 | | 856.5 | 0.78 | 20.7 | 1.40 | | |
| Beta NiOOH (3+ Portion) | 854.6 | 9.2 | 1.40 | | 0.70 | 855.3 | 8.3 | 1.50 | | 0.36 | 855.7 | 6.4 | 1.40 | | 856.5 | 0.78 | 13.8 | 1.40 | | e |
| Beta NiOOH (2+ Portion) | 854.9 | 2.5 | 1.12 | | 0.77 | 855.7 | 15.1 | 2.25 | | 2.02 | 857.7 | 1.0 | 1.59 | | 860.5 | 2.79 | 0.5 | 1.06 | | e |

| Compound | Peak 5 (eV) | % | Δ Peak 5 – Peak 4 (eV) | Peak 5, FWHM, 10-eV pass energy | Peak 5, FWHM, 20-eV pass energy | % | Peak 6 (eV) | Δ Peak 6 – Peak 5 (eV) | Peak 6, FWHM, 10-eV pass energy | Peak 6, FWHM, 20-eV pass energy | Peak 7 (eV) | % | Δ Peak 7 – Peak 6 (eV) | Peak 7, FWHM, 10-eV pass energy | Peak 7, FWHM, 20-eV pass energy | |
|---|---|---|---|---|---|---|---|---|---|---|---|---|---|---|---|---|
| Ni metal from Ref. [7] | | | | | | | | | | | | | | | | bd |
| Ni metal – new line-shape | | | | | | | | | | | | | | | | cd |
| NiO | 866.3 | 3.9 | 2.38 | 2.60 | 2.44 | | | | | | | | | | | |
| Ni(OH)2 | 861.5 | 39.2 | 1.00 | 4.64 | 4.65 | | | | | | | | | | | |
| Gamma NiOOH | 857.8 | 8.7 | 1.33 | 1.90 | | 3.7 | 866.5 | 4.96 | 3.08 | 3.01 | 864.4 | 11.4 | 3.38 | 4.40 | | |
| Beta NiOOH (3+ Portion) | 857.8 | 5.8 | 1.33 | 1.90 | | 23.3 | 861.0 | 3.20 | 4.00 | | 864.4 | 7.6 | 3.38 | 4.40 | | e |
| Beta NiOOH (2+ Portion) | 861.5 | 13.1 | 1.00 | 4.64 | | 15.6 | 861.0 | 3.20 | 4.00 | | | | | | | e |

[a] Binding energies are significant to 0.1 eV but an additional figure is added because energy splittings are much more accurate than the absolute binding energies.
[b] Asymmetric peak shape for peak 1 defined by standard nickel metal sample, CasaXPS peak shape parameter = A(0.4,0.55,10)GL (30).
[c] Asymmetric peak shape for peak 1 defined by standard nickel metal sample, CasaXPS peak shape parameter = LA(1.1,2.2,10).
[d] Metal peak is corrected to Au 4f7/2 set to 83.95 eV. All other peaks are charge corrected to C 1s (C–C, C–H, adventitious carbon) set to 284.8 eV.
[e] Beta NiOOH has a ratio of 2 : 1 Ni(III) : Ni(II). Peak percentages for the 3+ and 2+ portions for Beta NiOOH total 100%.
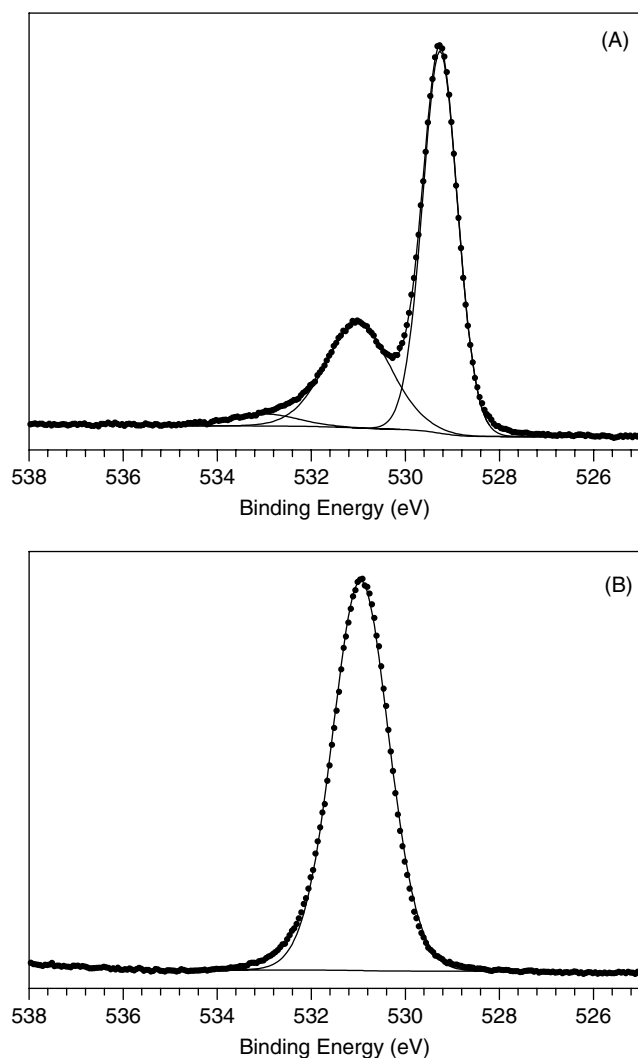
**Figure 1.** O 1s spectra of (A) NiO and (B) Ni(OH)$_2$.



**Figure 2.** Ni 2p thin oxide film spectra. (A) Shirley background under only the Ni 2p$_{3/2}$ portion of the spectrum. (B) Shirley background under the entire Ni 2p spectrum. (C) Shirley background under the entire Ni 2p spectrum with an offset on the higher binding energy endpoint.

loss peaks for Ni metal and an empirical fit of the NiO line shape from the parameters derived from the standard sample presented in Table 1. The binding energy differences, FWHM and area ratios are constrained for each species. The absolute binding energy values were allowed to vary by $\pm 0.2$ eV to allow for error associated with charge referencing to adventitious C 1s.

A Shirley background was applied across the 2p$_{3/2}$ portion of the spectrum (Fig. 2(A)). This initial fitting works reasonably well for most of the spectral area except near the higher energy satellite peaks (arrow 1, Fig. 2(A)) where there exists some overlap with the metal 2p$_{1/2}$ main peak. If a Shirley background is applied to the full 2p (2p$_{3/2}$ and 2p$_{1/2}$) envelope (Fig. 2(B)) fitting of the satellite region improves slightly (arrow 2, Fig. 2(B)).

If the higher energy end of the background is adjusted with a slight offset the fitting can be improved greatly (Fig. 2(C)). The quantitative results for the three different backgrounds from Fig. 2 show only a difference of a few tenths of a percent. It is necessary during spectral acquisition to use a window of sufficient width to accurately assess the end of the Ni 2p$_{1/2}$ envelope for positioning the background endpoint (arrow 3, Fig. 2(C)). A window from 848.0 eV to 890.0 eV is generally sufficient.

On examination of the standard NiO spectra it can be seen why a high binding energy offset to the Shirley background is effective.
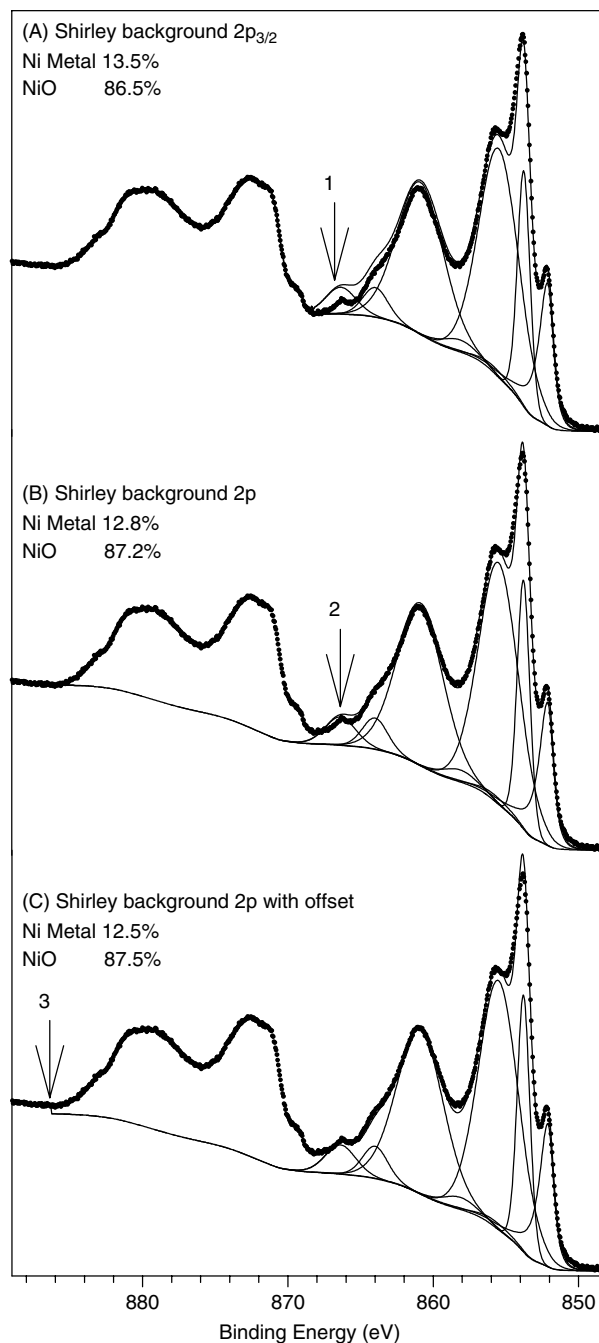
Figure 3(A) and 3(B) shows a normal Shirley background applied to the 2p$_{3/2}$ portion of the spectrum, a background applied to the entire 2p envelope, and a third background with a slight offset. The latter lines up well with the 2p$_{3/2}$ only background while the full 2p envelope background without the offset intersects the middle portion of the spectrum (Fig. 3(B)). This is also the case for the Ni(OH)$_2$ standard (Fig. 3(C) and 3(D)). These results justify the use of the offset for these samples especially where the 2p$_{3/2}$ − 2p$_{1/2}$ valley is obscured by spectral overlap (as is the case here (Fig. 1) and in Case 2). A Shirley background was chosen
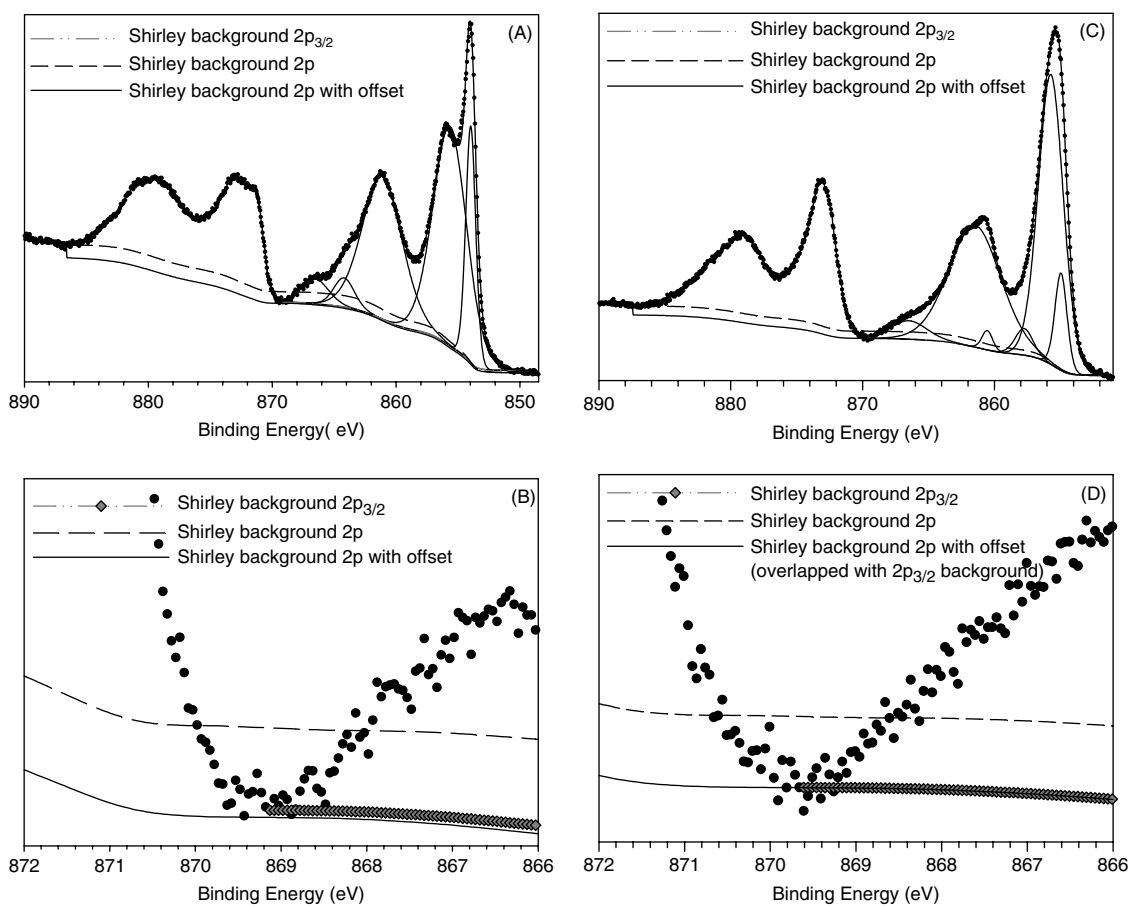
**Figure 3.** Ni 2p spectra of NiO (A) and (B) and Ni(OH)$_2$ (C) and (D) showing three different Shirley background configurations. Figures (B) and (D) provide detail on the backgrounds at the low intensity region between the Ni 2p$_{3/2}$ and Ni 2p$_{1/2}$ portions of the spectra for NiO and Ni(OH)$_2$, respectively. The fitted peaks use the Shirley background across the 2p$_{3/2}$ portion of the spectra.

for use here as it is considered to be good compromise between the physically unrealistic linear background and the physically realistic Tougaard background, which is difficult to employ in many practical situations.[25]

The appropriate background offset was determined using an iterative approach while monitoring a residual plot of the 2p$_{3/2}$ area. Unfortunately one cannot monitor the residual STD values or chi-squared values supplied by most fitting software packages as these values include the unfitted area under the 2p$_{1/2}$ portion of the spectra. If a value that includes only the 2p$_{3/2}$ portion of the spectrum can in the future be calculated this would remove some (small) uncertainty in the fitting. However, the quantitative values obtained with the offset background will still be an improvement over those not employing an offset.

With spectra that are charge corrected to C 1s set to 284.8 eV, it has been found in some cases that the binding energy range for the metal peak may have to be widened somewhat. Some differential charging of the oxide (and hydroxide) and metal may be found. Error inherent in the use of adventitious C as a charge reference, compared to referencing the metal peak for relatively conductive samples (as is the case here), may play a role. However, the metal peak here is well resolved and can be fitted without concern as to its exact binding energy. With nickel powder samples, or samples where differential charging may be of concern, mounting of samples on a nonconductive adhesive has worked well. With inhomogeneous samples, the use of nonconductive tape for mounting in conjunction with the use of the charge neutralizer system produces an equal potential across the surface of the sample. This effectively isolates the sample, making charging of all components relatively comparable.[26]

### Case 2: Ni Metal, NiO and Ni(OH)$_2$

For nickel compounds the spin-orbit splitting of the 2p$_{3/2}$ and 2p$_{1/2}$ is, in most cases large enough, so that only the more intense 2p$_{3/2}$ signal need be considered. However, overlap of the high binding energy satellite structure from Ni(OH)$_2$ with the 2p$_{1/2}$ metal line, which is composed of an asymmetric main line and contributions from plasmon loss structure, can make the definition of an appropriate spectral background problematic.

Spectral fitting of metal, oxide and hydroxide spectral components to XPS data measured for systems containing all three species is shown in Fig. 4. Fitting parameters are the same as described in Case 1 with the inclusion of the components for Ni(OH)$_2$ (Table 1). For the INCO (Type 123) nickel powder used for alloying and sintered powder metallurgical operations shown in Fig. 4(A), little to no offset in the Shirley background is needed. Quantitative analysis of this spectrum derives the Ni being present as 36.3% metal, 32.7% oxide and 31.0% hydroxide.

For the ultrafine nickel powder, Fig. 4(B), a larger offset, similar in magnitude to that used for the pure NiO and Ni(OH)$_2$ samples shown in Fig. 3, is needed. As in case 1, an iterative approach is used
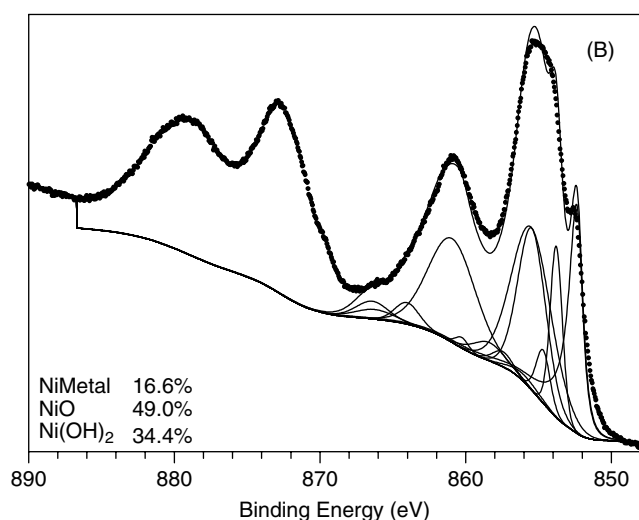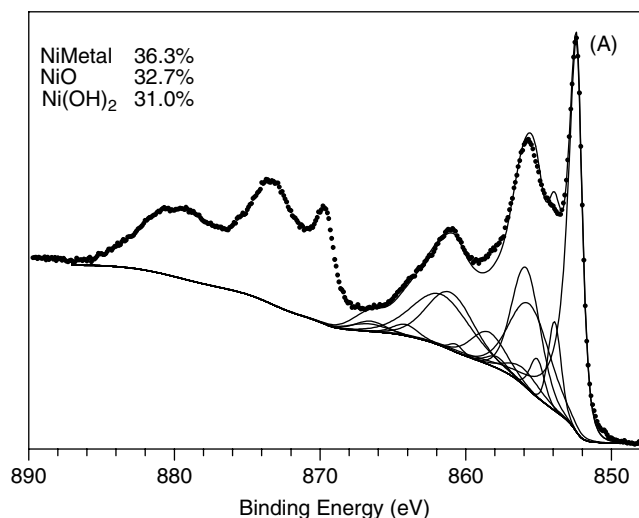
**Figure 4.** Ni 2p spectra of INCO (Type 123) nickel powder (A) and an ultrafine nickel powder (B) A Shirley background under the entire Ni 2p spectrum with an offset on the higher binding energy endpoint is used for both spectra.

**Figure 5.** Ni 2p$_{3/2}$ portions of the Ni 2p spectra of $\gamma$-NiOOH (A) and $\beta$-NiOOH (B). The Ni(III) spectral shape for $\beta$-NiOOH is modeled after that of the $\gamma$-NiOOH spectrum and the Ni(II) components are modeled after that of Ni(OH)$_2$.

to determine this. Quantitative analysis results in a reduced metal component (16.6%) and increased oxide (49.0%) and hydroxide (34.4%). For the ultrafine Ni powder (Fig. 4(B)) the larger offset does start to significantly affect the quantitative numbers compared to the same analysis with no background offset which results in Ni being present as 18.6% metal, 44.7% oxide and 36.7% hydroxide.

### Case 3: $\gamma$-NiOOH and $\beta$-NiOOH

Data for $\gamma$-NiOOH and $\beta$-NiOOH are based on that originally presented by Grosvenor et al.[7] The $\gamma$-NiOOH spectral fits (Fig. 5(A) and Table 1) are duplicated from Ref. [7]. Reference [7] shows the $\beta$-NiOOH spectrum to be broadened slightly at the lower binding energy suggesting the presence of the decomposition product, Ni(II). This was confirmed by the approximately 2:1 OH$^-$: O$^{2-}$ ratio (from the O 1s spectrum) suggesting Ni$_3$(OH)$_4$O$_2$. An Ni(II) component was added to the fit of the Ni data but the satellite contributions were not included.[7] Figure 5(B) shows a revised fit of the Ni(III) and Ni(II) components. The Ni(III) spectral shape is based on the $\gamma$-NiOOH spectrum and the Ni(II) components
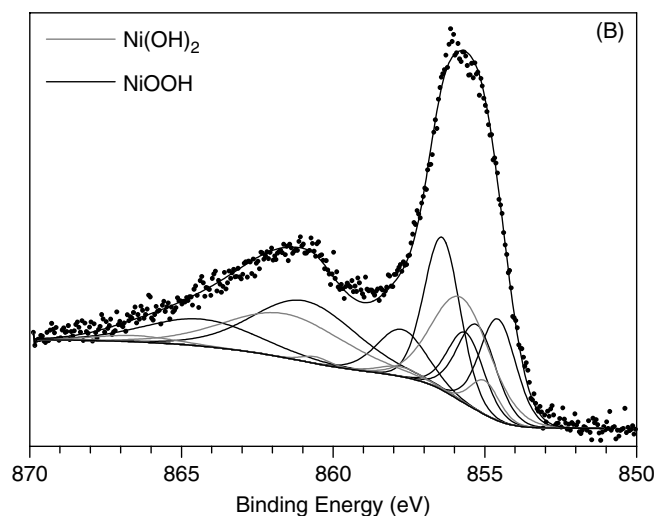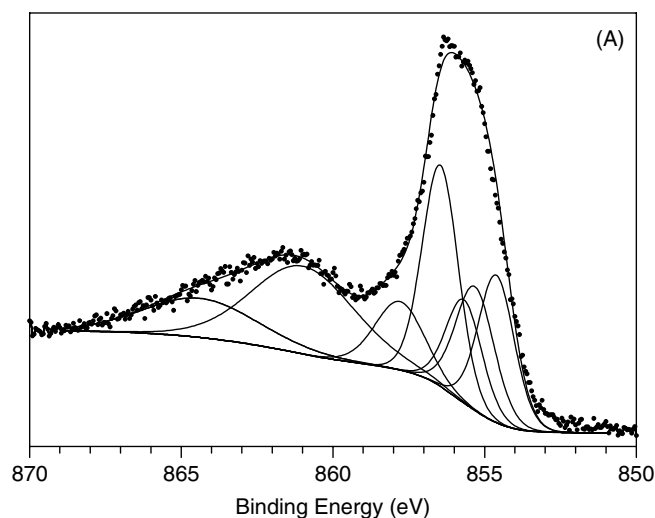
are based on Ni(OH)$_2$. The fitting parameters were constrained (Fig. 5(B) and Table 1) to give a 2:1 Ni(III):Ni(II) ratio as required by the stoichiometry of Ni$_3$(OH)$_4$O$_2$ as described in Refs [7,15].

### Case 4: Spectral subtractions

If the sample contains a large amount of Ni metal, particularly in thin film samples (<2 nm), spectral subtractions can be an appropriate methodology for the determination of the other nickel species present.[13,14] Figure 6(A) provides the Ni 2p spectrum from a nickel metal surface covered by a thin nickel oxide film grown on exposure to high-purity O$_2$ gas (1 Torr, 300 °C, 1 min). The intensity of the nickel metal spectral component makes it difficult to examine the nature of the oxidized nickel species however, removal of the nickel metal component by spectral subtraction (Fig. 6(B)) results in a rather broad peak. Subtraction is carried out after normalizing to the peak height of the main metal line for both the thin oxide film spectrum and the standard metal spectrum. As the resulting broad peak does not exhibit the expected multiplet splitting associated with Ni(II) as found in NiO, a further species is
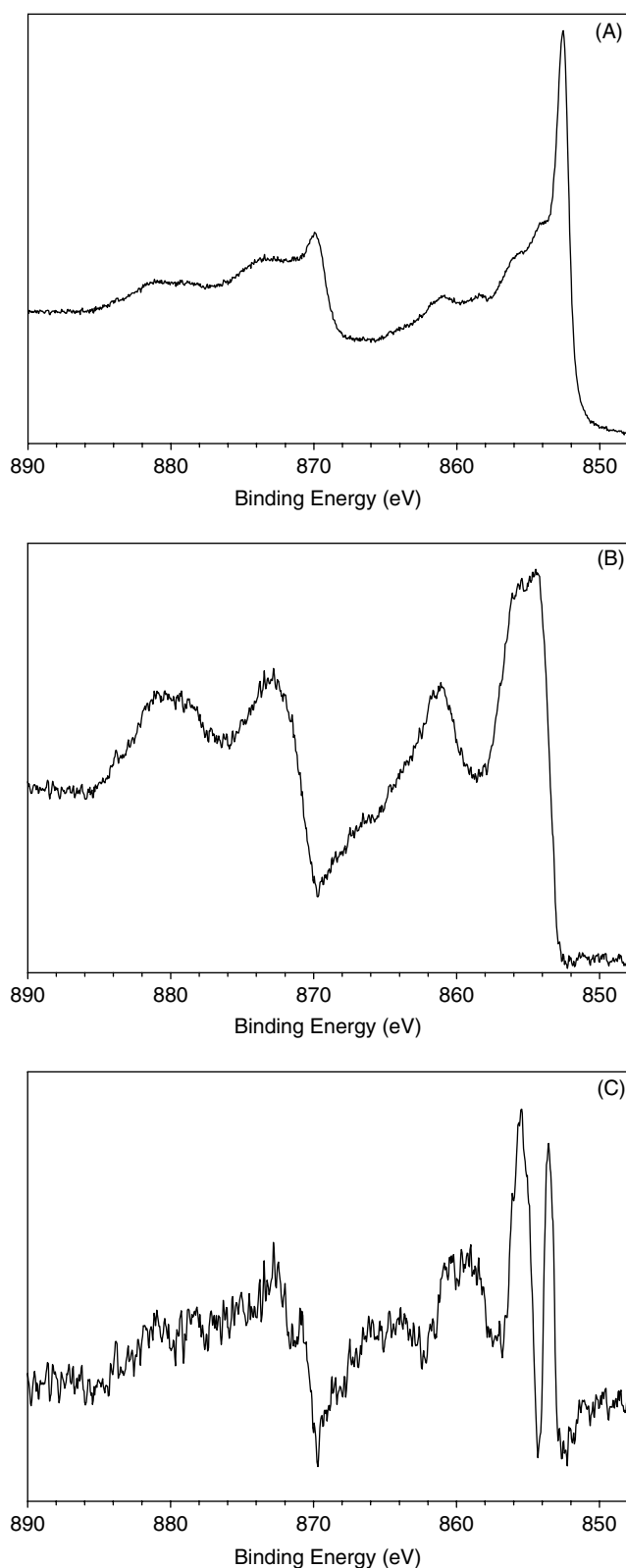
**Figure 6.** Ni 2p spectra from (A) Ni metal surface covered by a thin NiO film: (B) after subtraction of the metal spectral components and (C) after subtraction of the metal and NiO spectral components.

proposed. The subtraction of a NiO contribution leaves a residual spectra peak of shape similar to that of $\gamma$-NiOOH, an Ni (III)

containing compound (Fig. 6(C)). The sharp peak found at lower binding energy might result from a combination of remaining Ni metal signal, not completely removed by spectral subtraction, and the Ni−S interactions ($\approx$853 eV). S is a contaminant in bulk Ni that migrates to the surface during heating and was detected in the survey scan analysis.

### Case 5: Quantification of nickel metal, NiO and Ni(OH)$_2$ through comparative analysis of Ni 2p and O 1s

Initial analyses using relative sensitivity factors (RSFs) developed for the Kratos XPS gave Ni : O relative atomic percentages for a NiO powder standard of 45.5 : 54.5. The same spectra processed using Scofield RSFs gave Ni : O atomic ratios of 54.0 : 46.0. Neither RSF values gave the desired 50 : 50 stiochiometry of NiO and this suggests that, for a more precise quantitation, RSF values derived from well-characterized standard materials must be used. With this objective the following approach was employed.

Using the Kratos RSF value for O (0.78), an analysis of a series of NiO samples (samples used to derive the data in Table 1) (seven region analyses from high-resolution spectra and four survey scan analyses) was undertaken. The RSF for Ni $2p_{3/2}$ was then varied to obtain a 1 : 1 stoichiometry resulting in an RSF value of $2.7 \pm 0.4$. A similar analysis was carried out for Ni(OH)$_2$ (five region analyses and four survey scan analyses) resulting in an RSF value of $2.6 \pm 0.7$. Only the Ni $2p_{3/2}$ portion of the spectrum was used for these calculations as it has been found that the application of a Shirley background across the entire 2p envelope sometimes results in cutting off of the spectrum at valley between the $2p_{1/2}$ and $2p_{3/2}$ peaks. The O 1s peak RSF was kept fixed, as it has been found to be accurate for other test samples (e.g. silicon dioxide).

Combining the two results gives $2.7 \pm 0.5$. Although this value is comparable to the Kratos RSF value of 2.696, the large uncertainty is unacceptable. This may result from (i) adsorption/reaction with H$_2$O and O containing carbonaceous materials on the surface of the standards; (ii) use of the Shirley background which excludes a significant portion of the true intensity calculated by Scofield[25]; (iii) beam damage/reduction of the compounds; (iv) noise in the spectra (particularly the low resolution survey scans); (v) variability in picking baseline endpoints (again more of a problem for low resolution survey scans). However, comparison of the oxide/hydroxide percentages between the Ni 2p and O 1s spectra should provide reasonable agreement if no other O containing species are present in the sample. Unfortunately this is generally not the case for most samples taken from practical examples. At the least, air exposed samples will have some O functionality associated with adventitious C and possibly from adsorbed and/or reacted H$_2$O.

### Depth of analysis: thin film NiO and Ni(OH)$_2$

Analysis of thin films of NiO or Ni(OH)$_2$ often requires an estimation of film thickness. To this end, models of the O 1s and Ni 2p photoelectron intensity versus depth for both bulk Ni(OH)$_2$ and NiO are presented in Figs 7(A) and 7(B). The IMFPs were calculated using the NIST Electron Inelastic Mean Free Path Database (Version 1.1) software[27] using the predictive formulae routines from Tanuma, Powell and Penn.[28] For Ni(OH)$_2$ and NiO, densities of 4.15 and 6.67 g cm$^{-3}$ were used. There is a paucity of band gap data available for these calculations. NiO band gap values of 3.65 eV[29] and 3.55 eV[30] were averaged to give a value of 3.6 eV. This results in NiO IMFP values of 1.798 nm and 1.330 nm
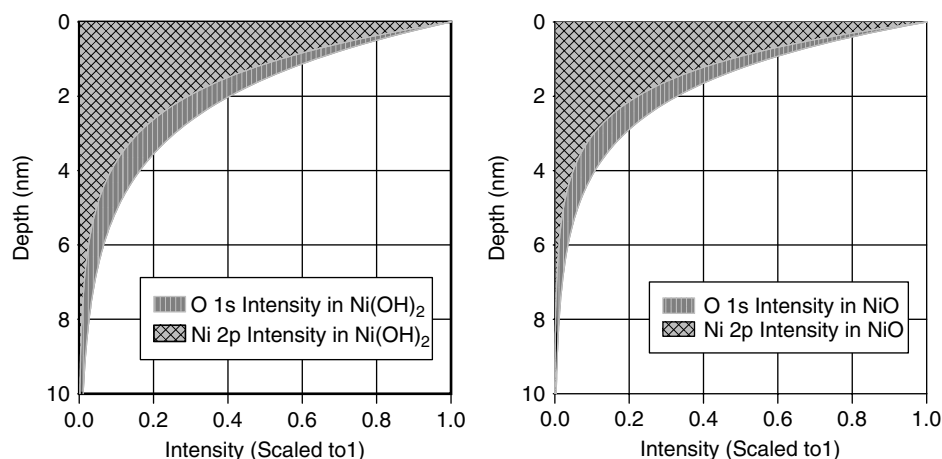
**Figure 7.** Models of the O 1s and Ni 2p photoelectron intensity as a function of depth for Ni(OH)$_2$ (left) and NiO (right).

for O 1s and Ni 2p photoelectrons, respectively. The band gap data for Ni(OH)$_2$ is less precise with values for thin film Ni(OH)$_2$ of 3.05 eV[31] and 2.5 eV[32] to give an average of 2.78 eV. This results in Ni(OH)$_2$ IMFP values of 2.206 nm and 1.628 nm for O 1s and Ni 2p photoelectrons, respectively.

Using these IMFP values ($\lambda$), the intensity $I(d)$ of photoelectrons at a depth ($d$) into the solid can be calculated with the following formula:

$$I(d) = I_0 \cdot e^{(-d/\lambda)} \tag{1}$$

where $I_0$ is the primary intensity (set to 1). The appropriate IMFP values can then be applied for film thickness analysis using routines such as QUASES[33] or for oxide depth ($d$) calculations of the type used by Carlson[34] and Strohmeier[14,35] defined as follows:

$$d = \lambda_{ox} \ \sin 2 \ \ln\{[(N_m \, \lambda_m \, I_{ox})/(N_{ox} \, \lambda_{ox} \, I_m)] + 1\} \tag{2}$$

where 2 is the photoelectron takeoff angle, $I_{ox}$ and $I_m$ are the area percentages of the oxide and metal peaks from the high-resolution spectrum, and $N_m$ and $N_{ox}$ are the volume densities of the metal atoms in the metal and oxide, respectively.

Considering an assumed uniformly mixed oxide/hydroxide thin film with known oxide, hydroxide and metal concentrations (using the fitting procedures in Case 2) and given $N_m/N_{ox}$ and $N_m/N_{hydrox}$ values of 1.70 and 3.39 for NiO and Ni(OH)$_2$, respectively, Eqn 2 can be modified to include weighted averages of the oxide/hydroxide IMFP and volume density ratio components as follows:

$$d = \lambda_{ox:hydrox} \ \sin 2 \ \ln\{[N_m \, \lambda_m \, (I_{ox} + I_{hydrox})/ $$
$$ (N_{ox:hydrox} \, \lambda_{ox:hydrox} \, I_m)] + 1\} \tag{3}$$

Using this calculation a thin film with 40.0% oxide, 37.5% hydroxide and 12.5% metal would have a film thickness of 3.6 ± 0.2 nm. As expected, this gives a thicker film value than that for the similar oxide only film in case 1 (12.5% metal, 87.5% oxide, 3.2 ± 0.2 nm, thickness confirmed by QUASES and NRA analyses) which has the same metal peak area as that for the hypothetical oxide/hydroxide film above.

## Conclusion

XPS analysis of the main Ni 2p peak shapes of Ni metal, oxide, oxy-hydroxides, and hydroxide is challenging due to the complexity of multiplet splitting, shake-up and plasmon loss structure. Practical curve fitting procedures for the various nickel chemical states in model compounds has been presented. The case studies presented show a series of practical procedures for the identification of nickel species and the quantitative measurement of these chemical states in real samples. These procedures have been found to be consistently reproducible across a wide range of samples. Problems with variability of RSF values have been identified and discussed. Estimates of IMFP values of NiO and Ni(OH)$_2$ usable for thin film thickness analysis are presented.

## References

[1] C. D. Wagner, A. V. Naumkin, A. Kraut-Vass, J. W. Allison, C. J. Powell, J. R. Rumble Jr, *NIST Standard Reference Database 20, Version 3.4 (Web Version)*, **2003**, http:/srdata.nist.gov/xps/.

[2] J. F. Moulder, W. F. Stickle, P. E. Sobol, K. D. Bomben, in *Handbook of X-ray Photoelectron Spectroscopy* (Ed.: J. Chastain), Perkin-Elmer Corp: Eden Prairie, **1992**.

[3] M. C. Biesinger, C. Brown, J. R. Mycroft, R. D. Davidson, N. S. McIntyre, *Surf. Interface Anal.* **2004**, *36*, 1550.

[4] H. W. Nesbitt, D. Banerjee, *Am. Mineral.* **1998**, *83*, 305.

[5] D. Banerjee, H. W. Nesbitt, *Geochim. Cosmochim. Acta* **1999**, *63*, 3025.

[6] A. P. Grosvenor, B. A. Kobe, M. C. Biesinger, N. S. McIntyre, *Surf. Interface Anal.* **2004**, *36*, 1564.

[7] A. P. Grosvenor, M. C. Biesinger, R. St. C. Smart, N. S. McIntrye, *Surf. Sci.* **2006**, *600*, 1771.

[8] H. A. E. Hagelin-Weaver, J. F. Weaver, G. B. Hoflund, G. N. Salaita, *J. Electron Spectrosc. Relat. Phenom.* **2004**, *134*, 139.

[9] R. P. Gupta, S. K. Sen, *Phys. Rev. B* **1974**, *10*, 71.

[10] R. P. Gupta, S. K. Sen, *Phys. Rev. B* **1975**, *12*, 12.

[11] H. A. E. Hagelin-Weaver, J. F. Weaver, G. B. Hoflund, G. N. Salaita, *J. Alloys Compd.* **2005**, *389*, 34.

[12] M. W. Roberts, R. St. C. Smart, *J. Chem. Soc., Faraday Trans.* **1984**, *80*, 2957.

[13] A. F. Carley, S. D. Jackson, J. N. O'Shea, M. W. Roberts, *Surf. Sci.* **1999**, *440*, L868.

[14] B. P. Payne, A. P. Grosvenor, M. C. Biesinger, B. A. Kobe, N. S. McIntyre, *Surf. Interface Anal.* **2007**, *9*, 582.

[15] L. M. Moroney, R. St. C. Smart, M. W. Roberts, *J. Chem. Soc., Faraday Trans.* **1983**, *79*, 1769.

[16] N. S. McIntyre, D. G. Zetaruk, D. Owen, *Appl. Surf. Sci.* **1978**, *2*, 55.

[17] L. J. Matienzo, L. I. Yin, S. O. Grim, W. E. Swartz, *Inorg. Chem.* **1973**, *12*, 2762.

[18] A. F. Carley, P. R. Chalker, M. W. Roberts, *Proc. R. Soc. London, Ser. A* **1985**, *399*, 167.

[19] D. J. Miller, M. C. Biesinger, N. S. McIntyre, *Surf. Interface Anal.* **2002**, *33*, 299.

[20] N. Fairley, http://www.casaxps.com, © Casa software Ltd. **2005**.

[21] P. R. Norton, G. L. Tapping, J. W. Goodale, *Surf. Sci.* **1977**, *65*, 13.

[22] B. P. Payne, M. C. Biesinger, N. S. McIntyre, *J. Electron Spectrosc. Relat. Phenom.* **2009**, submitted.

[23] C. Benndorf, C. Nöbl, F. Thieme, *Surf. Sci.* **1982**, *121*, 249.

[24] A. F. Carley, S. Rassias, M. W. Roberts, *Surf. Sci.* **1983**, *135*, 35.

[25] G. C. Smith, in *Handbook of Surface and Interface Analysis* (Eds: J. C. Riviere, S. Myhra), Marcel Dekker, Inc.: New York, **1998**, pp 184.

[26] B. J. Tielsch, J. E. Fulghum, D. J. Surman, *Surf. Interface Anal.* **1996**, *24*, 459.

[27] *NIST Electron Inelastic Mean Free Path Database (Version 1.1)* © **2000**, U.S. Secretary of Commerce.

[28] S. Tanuma, C. J. Powell, D. R. Penn, *Surf. Interface Anal.* **1991**, *17*, 927.

[29] Y. P. Wang, J. W. Zhu, L. L. Zhang, X. J. Yang, X. Wang, *Spectrosc. Spect. Anal.* **2006**, *26*, 690.

[30] G. Boschloo, A. Hagfeldt, *J. Phys. Chem. B* **2001**, *105*, 3039.

[31] H. G. Jang, C. J. Park, H. S. Kwon, *Electrochim. Acta* **2005**, *50*, 3503.

[32] S. Fujimoto, H. Tsuchiya, M. Sakamoto, K. Asami, Proceeding of the 201st Meeting of the Electrochemical Society, Philadelphia, Pennsylvania, 12–17 May, **2002**, 278.

[33] S. Tougaard, QUASES™, Software for Quantitative XPS/AES of Surface Nano-Structures by Analysis of the Peak Shape and Background, www.quases.com, **2000**.

[34] T. A. Carlson, G. E. McGuire, *J. Electron Spectrosc. Relat. Phenom.* **1972/73**, *1*, 161.

[35] B. R. Strohmeier, *Surf. Interface Anal.* **1990**, *15*, 51.